HHS Public Access

Author manuscript

Nat Neurosci. Author manuscript; available in PMC 2015 October 01.

Published in final edited form as:

Nat Neurosci. 2015 April ; 18(4): 501–510. doi:10.1038/nn.3960.

Mitochondrial Control by DRP1 in Brain Tumor Initiating Cells

Qi Xie[1], **Qiulian Wu**[1], **Craig M. Horbinski**[2], **William A. Flavahan**[1], **Kailin Yang**[1,3], **Wenchao Zhou**[1], **Stephen M. Dombrowski**[4], **Zhi Huang**[1], **Xiaoguang Fang**[1], **Yu Shi**[1], **Ashley N. Ferguson**[5], **David F. Kashatus**[5], **Shideng Bao**[1,3], and **Jeremy N. Rich**[1,3]

[1]Departments of Stem Cell Biology and Regenerative Medicine, Lerner Research Institute, Cleveland Clinic, Cleveland, OH 44195

[2]Department of Pathology, University of Kentucky, Lexington, KY 40536

[3]Molecular Medicine, Cleveland Clinic Lerner College of Medicine of Case Western Reserve University, Cleveland Clinic, Cleveland, OH 44195

[4]Neurological Surgery, Cleveland Clinic, Cleveland, OH 44195

[5]Department of Microbiology, Immunology and Cancer Biology, University of Virginia, Charlottesville, VA 22908

Abstract

Brain tumor initiating cells (BTICs) coopt the neuronal high affinity GLUT3 glucose transporter to withstand metabolic stress. Here, we investigated another mechanism critical to brain metabolism, mitochondrial morphology. BTICs displayed mitochondrial fragmentation relative to non-BTICs, suggesting that BTICs have increased mitochondrial fission. The essential mediator of mitochondrial fission, dynamin-related protein 1 (DRP1), was activated in BTICs and inhibited in non-BTICs. Targeting DRP1 using RNA interference or pharmacologic inhibition induced BTIC apoptosis and inhibited tumor growth. Downstream, DRP1 activity regulated the essential metabolic stress sensor, AMP-activated protein kinase (AMPK), and AMPK targeting rescued the effects of DRP1 disruption. Cyclin-dependent kinase 5 (CDK5) phosphorylated DRP1 to increase its activity in BTICs, whereas Ca^{2+}–calmodulin-dependent protein kinase 2 (CAMK2) inhibited DRP1 in non-BTICs, suggesting tumor cell differentiation induces a regulatory switch in mitochondrial morphology. DRP1 activation correlates with poor prognosis in glioblastoma, suggesting mitochondrial dynamics may represent a therapeutic target for BTICs.

INTRODUCTION

Glioblastomas rank among the most lethal of human cancers with current therapies offering only palliation[1]. Glioblastomas display striking intertumoral heterogeneity in transcriptional

Correspondence should be addressed to: Jeremy N. Rich, MD, MHSc, Department of Stem Cell Biology and Regenerative Medicine, Lerner Research Institute, Cleveland Clinic, 9500 Euclid Ave., NE3, Cleveland, OH 44195, Telephone: (216) 636-0790; Facsimile: (216) 636-5454, drjeremyrich@gmail.com.

The authors declare no competing interests.

programs and genetic lesions[2, 3], but glioblastomas also phenocopy aberrant organ systems with intratumoral heterogeneity within the neoplastic compartment derived from genetic and epigenetic forces, leading to cellular hierarchies with self-renewing BTICs at the apex[4–6]. Normal neural progenitor cells (NPCs) are functionally defined by self-renewal and differentiation into relevant lineages[7]. BTICs share these features but are distinguished by their frequency, proliferation, aberrant expression of differentiation markers, chromosomal abnormalities, and tumor formation. While BTICs remain controversial due to unresolved issues over cell-of-origin and purification, BTICs have generated substantial interest due to their resistance to conventional therapies, evasion of anti-tumor immune responses, promotion of tumor angiogenesis and invasion into normal tissues[8–11].

Evolving models of cancer hallmarks have integrated metabolism as an essential feature of cellular transformation[13]. Metabolic changes are not simply a result of oncogenesis, as mutations in key enzymes are primary tumor initiating lesions[13]. Isocitrate dehydrogenase 1 (IDH1) is mutated in the majority of low-grade gliomas and secondary glioblastomas leading to formation of an oncometabolite causing cellular dedifferentiation[14, 15]. However, most glioblastomas express wild type IDH1[14], suggesting potential alternative regulation of metabolism. Like most cancers, glioblastomas display derangement of metabolism to promote a shift towards glycolysis, known as the Warburg effect[16]. While all tumor cells display dysregulation of metabolic pathways, the differential growth patterns of BTICs suggest that these tumor subpopulations have metabolic features that distinguish them from the tumor bulk[17–20]. Recent studies suggest that the molecular machinery of nutrient sensation instructs the behavior of stem cells, particularly embryonic and hematopoietic stem cells[21]. As mitochondria represent the central metabolic organelle, mitochondria offer a potential link between cellular metabolism and differentiation state.

Mitochondria are highly dynamic organelles that synergize with the central cellular state[22]. To meet specific cellular demands of different cell types over time, cellular biogenesis is mediated through the dynamic mitochondrial fusion and fission. Mitochondrial dynamics are tightly coordinated in association with the cell cycle and state with complex structural and functional interactions leading to fusion and fission of mitochondria to alter the balance of oxidative-phosphorylation, eliminate damaged mitochondrial components (e.g. mtDNA), and regulate reactive oxygen species (ROS)[22]. Embryonic stem cell maintenance and lineage commitment is regulated by mitochondrial dynamics[23–25]. Mitochondrial fission removes damaged mitochondrial components through mitophagy but excessive fission may contribute to Parkinson's and Huntington's diseases[22]. Cancers, including glioblastomas, have increased rates of mitochondrial fission[26–32]. Thus, mitochondria fission may be related to stem cell biology, beneficial for cancer and destructive in normal brain. Mitochondria dynamic fusion and fission mediators have been closely linked to cell fate determination and development[35]. Acquired alterations in these mitochondrial regulators occur in neurodegenerative diseases, vascular disorders, and cancer. Inhibitors of mitochondrial fission [e.g. mitochondrial division inhibitor-1 (Mdivi-1)] may ameliorate neurodegenerative diseases and reduce the cardiotoxicity of chemotherapy[36, 37].

Here, we interrogated the role of mitochondrial form and functional control within the cellular hierarchy of the most common primary intrinsic brain tumor, glioblastoma, using

validated and well characterized models reflecting the tumor hierarchy[8, 9, 19, 38, 39]. As metabolic control offers a potential node upon which diverse extrinsic and intrinsic cellular signaling pathways converge, these studies may inform the development of novel anti-cancer therapy.

RESULTS

BTICs display fragmented mitochondrial morphology

To investigate mitochondrial control in BTICs, we isolated functionally validated matched BTIC and non-BTIC cell populations from patient-derived xenografts. Sphere culture is often used to enrich for BTICs, but this methodology prevents the prospective comparison of BTICs and non-BTICs needed for these studies. Using cell surface markers immediately upon tumor harvesting prevents the loss of information as cell surface markers mediate interactions with the tumor microenvironment. Glioblastomas display substantial intertumoral heterogeneity so it is not surprising that enrichment markers for BTICs are not universally informative. CD133 (PROMININ1) is the most widely used BTIC marker but also controversial due to its technical challenges and variable expression patterns, but we and others have repeatedly demonstrated in our models that CD133 used immediately on patient tumor specimens or xenografts is informative of functional BTICs as measured by stem cell marker expression, in vitro and in vivo limiting dilution, including the models included in this study[4, 8, 9, 19, 38, 39]. Therefore, our claim of BTIC identity is based on functional criteria, not markers. As culture and xenograft conditions can induce drift, we used both xenografts and cultures at early passage (<5 passages). For maintenance, BTICs and non-BTICs were cultured separately in optimal media, but for every experiment, all cells were cultured under identical conditions and media. Validation of the cellular hierarchy was revalidated functionally (data not shown).

Using this selection system, we compared the mitochondrial morphology of BTICs with non-BTICs using a mitochondrial marker (translocase of outer mitochondrial membranes 20 kDA, TOM20) and three-dimensional Imaris image reconstruction of images obtained from confocal microscopy (Bitplane, South Winsor, CT). Mitochondria in BTICs were more fragmented and less tubular than matched non-BTICs (Fig. 1a, b). Consistent with these observations, electron microscopic examination confirmed shorter, rounded mitochondria in BTICs compared with elongated, tubular structures in non-BTICs (Fig. 1c, d). Taken together, these findings suggest that mitochondrial fragmentation may be a distinctive feature of BTICs.

DRP1 phosphorylation controls BTIC mitochondrial morphology

Mitochondrial length is determined by the competitive balance between central mediators of mitochondrial fission and fusion. A dynamin-like protein, DRP1 (dynamin-related protein 1), mediates mitochondrial fission while MFN1 (mitofusin 1) and MFN2 are required for outer membrane fusion, and OPA1 (optic atrophy 1) is required for inner membrane fusion[22]. Based on differences in mitochondrial length, we interrogated the expression levels of these proteins. No consistent differences in whole cell protein levels of central mediators between matched BTICs and non-BTICs isolated from short-term patient-derived xenografts

were detectable (Supplementary Fig. 1), suggesting possible regulation at the post-translational level.

Phosphorylation of DRP1^{S616} enhances DRP1 activity, whereas phosphorylation of DRP1^{S637} represses function[33, 34]. We quantified levels of phosphorylated DRP1 at DRP1^{S616} and DRP1^{S637} in matched cultures of BTICs and non-BTICs from short-term xenografts by immunoblot (Fig. 2a). In every model tested, BTICs displayed strikingly elevated activating DRP1 phosphorylation (S616) and significantly down-regulated inhibitory DRP1 phosphorylation (S637) levels compared to matched non-BTICs. To address the possible concern regarding CD133 as a marker, we used an alternative marker (CD15; stage-specific embryonic antigen 1, SSEA1), which has been suggested as marker of BTICs[40]. In confirmation of our results with CD133, SSEA1 positive cells displayed an identical pattern of activated DRP1 relative to non-BTICs (Fig. 2b). For yet an additional confirmation of specific activation of DRP1 in BTICs independent of the CD133 marker, we demonstrated co-expression of phosphorylated DRP1 (S616) and BTIC markers, SOX2 and OLIG2, by immunofluorescence staining of human primary glioblastoma tissue sections (Fig. 2c). To additionally rule out an effect of culture conditions underlying these observations, we confirmed these results using BTICs and non-BTICs directly isolated from primary glioblastoma patient specimens without culture (Fig. 2d). To determine the relationship between cellular differentiation and DRP1 regulation, we induced differentiation in BTICs and found a marked switch in DRP1 phosphorylation from the activating modification (S616) to an inhibitory state (S637) (Fig. 2e), indicating that dynamic regulation of DRP1 by phosphorylation is important for BTICs self-renewal and differentiation. Collectively, these findings support DRP1 is hyperactivated in BTICs.

To determine whether DRP1 phosphorylation is critical for the mitochondria morphological change between BTICs and non-BTICs, we constructed gain-of-function DRP1 encoding both S616E (to mimic activating phosphorylation) and S637A (to block inhibitory phosphorylation) mutations. Over-expression of DRP1$^{S616E/S637A}$ in non-BTICs potently induced remodeling of mitochondria morphology (Fig. 3a–c). Mitochondria in non-BTICs transduced by lentivirus expressing mutated DRP1$^{S616E/S637A}$ became more fragmented and less elongated than cells that expressed a control vector (Fig. 3a–c). Furthermore, forced expression of DRP1$^{S616E/S637A}$ induced expression of some, but not all, selected core stem cell regulators (Fig. 3d) and repression of differentiation markers (Fig. 3e) compared to vector control. Expression of DRP1$^{S616E/S637A}$ was not sufficient to induce sphere or in vivo tumor formation (data not shown), suggesting that DRP1 activity alone is not sufficient to fully reprogram non-BTICs into BTICs. Together, these results demonstrate that hyperactivated DRP1 plays an essential role in mitochondrial fission in the tumor hierarchy.

DRP1 targeting decreases BTIC tumorigenecity

As induced differentiation of BTICs ablates the preferential hyperactivation of DRP1, suggesting a potential functional role of DRP1 in BTIC biology, we interrogated the requirement for DRP1 function in BTIC maintenance. We developed two independent, non-overlapping small hairpin RNA (shRNA) lentiviral constructs to knockdown DRP1 (designated hereafter as shDrp1#1 and shDrp1#2) compared to a control shRNA sequence

that does not target mammalian mRNA, which serves to rule out off target effects (non-targeting control, NT shRNA). *Drp1* shRNAs significantly reduced DRP1 protein expression levels on immunoblot (Fig. 4a). We then examined the phenotypic consequences of shRNA-mediated reduction of DRP1 expression. Silencing *Drp1* significantly decreased the growth of two BTIC models (Fig. 4a), whereas there was no effect on non-BTICs or human NPCs (Supplementary Fig. 2), further supporting the preferential requirement for DRP1 in BTICs. To determine whether targeting DRP1 also influences tumorsphere formation (a surrogate marker of self-renewal), we performed an in vitro limiting dilution assay in BTICs expressing non-targeting control shRNA or *Drp1*-directed shRNAs. Targeting *Drp1* resulted in a more than tenfold decrease in the frequency of sphere formation and fourfold or greater decrease in the sphere size (Fig. 4b, c). BTIC assessment requires in vivo tumor growth so we evaluated the potential antitumor effects of DRP1-directed interventions in vivo. BTICs transduced with either of two non-overlapping *Drp1*-targeting shRNAs or control NT shRNA were transplanted into the brains of immunocompromised mice. Animals bearing BTICs expressing shDrp1 displayed significantly reduced tumor formation and increased tumor latency and survival relative to those bearing BTICs expressing NT shRNA (Fig. 4d, e). Together, our data demonstrate that DRP1 is required to maintain the tumorigenic potential of BTICs and attenuation of DRP1 expression results in a loss of BTIC phenotypes, including proliferation, self-renewal, and tumor formation.

Pharmacologic blockade of DRP1 inhibits BTIC growth

Mitochondrial division inhibitor-1 (Mdivi-1), a selective cell-permeable small molecule inhibitor of the DRP1 GTPase activity, has emerged as a promising proof-of-concept therapeutic agent for stroke, myocardial infarction, and neurodegenerative diseases[36, 37]. Mdivi-1 has activity against established cancer cell lines in vitro[27–31] suggesting that inhibition of mitochondrial fission may be effective against tumor cells. Consistent with DRP1 knockdown experiments, blocking DRP1 activity by Mdivi-1 significantly decreased the growth of BTICs (Fig. 5a). Furthermore, Mdivi-1 treatment dramatically induced apoptosis measured by both Annexin V staining and PARP cleavage in BTICs but not non-BTICs or NPCs (Fig. 5b, 5c and data not shown). We validated the effects of Mdivi-1 treatment on mitochondrial morphology both in vitro (Supplementary Fig. 3a) and in vivo (Supplementary Fig. 3b).

Next, we sought to evaluate the potential antitumor effects of Mdivi-1 in vivo. We orthotopically implanted BTICs into the brains of immunocompromised mice. Three days after implantation, mice were treated for five days by tail vein injection with Mdivi-1 or vehicle control (DMSO). Mdivi-1 treatment increased tumor latency and survival with no evidence of toxicity (Fig. 5d and data not shown). Taken together, our findings support the efficacy of Mdivi-1 against BTICs growth and tumor formation, offering a novel paradigm into targeting stem-like brain tumor cells.

DRP1 inhibition induces AMPK activation in BTICs

Based on the role of DRP1 in controlling mitochondrial fission, we investigated BTIC metabolism within the context of disrupting DRP1 expression using the Seahorse cell

mitochondrial stress test kit, which uses pharmacologic inhibitors and activators of mitochondrial function to measure mitochondrial respiration and proton excretion in real time. Initial basal respiration is disrupted by Oligomycin treatment to determine ATP production (and proton leak) followed Trifluorocarbonylcyanide Phenylhydrazone (FCCP) to stimulate maximal respiration followed by Antimycin A and Rotenone to inhibit all mitochondrial respiration. FCCP stimulates mitochondria respiration by uncoupling ATP synthesis from electron transport, while Oligomycin and Antimycin A inhibit respiration by inhibiting ATP synthase and oxidation of ubiquinol in the electron transport chain, respectively. DRP1 depletion dramatically decreased BTIC oxygen consumption rate (OCR), leading to mitochondrial dysfunction (Supplementary Fig. 4a).

AMP-activated protein kinase (AMPK) is a central cellular sensor of energy stress, suggesting a potentially critical role in determining the survival of cells under metabolic stress. Using a pharmacologic activator of AMPK, we found that AMPK activation decreased BTIC growth and induced caspase activation (Supplementary Fig. 4b, c), concordant with studies in glioma cell lines[41], phenocopying DRP1 targeting. We therefore interrogated a potential link to AMPK activation under DRP1 inhibition in BTICs. DRP1 inhibition by either shRNA knockdown (Fig. 6a) or treatment with Mdivi-1 (Fig. 6b) led to upregulation of AMPK activation, measured by increased phosphorylation of AMPKα. To determine if AMPK regulation may serve as a critical downstream mediator of DRP1, we interrogated the potential for rescuing the phenotype caused by DRP1 targeting. While knocking down AMPKα by itself had minimal effect on BTIC growth or neurosphere formation, targeting AMPKα expression in the context of DRP1 inhibition rescued both the BTIC growth defect (Fig. 6c) and compromised neurosphere formation capacity (Fig. 6d), which strongly supports AMPKα as a critical downstream mediator of BTIC response following DRP1 inhibition. Collectively, our results suggest that DRP1 serves as a critical node in the response of BTICs to metabolic stress through AMPK regulation.

CDK5 activates DRP1 in BTICs

To determine the molecular mechanism activating DRP1 in BTICs, we investigated potential kinases regulating the phosphorylation status of DRP1. Cyclin-dependent kinase 1 (CDK1) has been reported to phosphorylate DRP1 at Ser616[33]. CDK family kinases -- especially CDK1, CDK2 and CDK5 -- often share substrates. To determine if the CDKs regulate BTIC DRP1^{S616} phosphorylation, we treated BTICs with Roscovitine, a pan-CDK1/2/5 inhibitor, and determined that DRP1^{S616} phosphorylation was significantly reduced (Fig. 7a) with associated loss of fragmented mitochondrial morphology (Supplementary Fig. 5). In contrast, treatment with BMS-265246, a CDK inhibitor more specific for CDK1/2, did not alter DRP1^{S616} phosphorylation (Fig. 7b) or mitochondrial morphology (Supplementary Fig. 5), indicating that CDK5 might be the dominant regulating kinase responsible for DRP1^{S616} phosphorylation in BTICs. We screened the expression of the CDKs in matched BTICs and non-BTICs and found that both CDK1 and CDK5 were preferentially expressed by BTICs in multiple tumors (Fig. 7c).

To determine if CDK5 could directly phosphorylate DRP1, we performed an in vitro kinase assay with CDK5, its regulatory partner p25 and GST-DRP1 (wild type or S616A mutant)

and found that CDK5 directly phosphorylates DRP1 on the S616 site (Fig. 7d). RNA interference against CDK5, but not CDK1, resulted in specific diminished phosphorylation on DRP1^{Ser616} (Fig. 7e). We next interrogated the functional importance of CDK5 in the regulation of mitochondrial morphology using the mitochondria marker, TOM20. Targeting CDK5 expression by shRNA in two BTIC models resulted in significantly longer mitochondria fibers (Fig. 7f) and inhibition of proliferation and sphere formation (Supplementary Fig. 6). While a contribution from CDK1 cannot be completely ruled out, these results strongly suggest that CDK5, which is expressed in post-mitotic neurons and serves critical roles in brain development and neurodegenerative diseases, may be an upstream driver of mitochondrial fission and metabolic control in BTICs through direct activation of DRP1 (Supplementary Fig. 6c).

CAMK2 inhibits DRP1 in non-BTICs

To determine the inhibitory regulation of DRP1 in non-BTICs, we screened potential upstream regulators of the inhibitory phosphorylation event in non-BTICs (phospho-DRP1^{S637}). Calcium/calmodulin-dependent protein kinase type 1 (CAMK1) has been previously reported to phosphorylate DRP1^{S63742}, so we targeted global CAMK function by a pan-CAMK pharmacologic inhibitor, KN93. We found downregulation of DRP1^{S637} phosphorylation in non-BTICs upon KN93 treatment (Supplementary Fig. 7a), but phospho-DRP1^{S637} was also compromised by treatment with a CAMK2-specific inhibitor, Autocamptide-2 Related Inhibitor Peptide (AIP) (Supplementary Fig. 7b). These results are consistent with the observation that expression levels of CAMK2 are higher in non-BTICs, while CAMK1 does not display preferential expression between BTICs and non-BTICs (Supplementary Fig. 7c).

We next interrogated the functional importance of CAMK2 in the regulation of mitochondrial morphology. AIP treatment, inhibiting CAMK2, in non-BTICs induced a shift towards fragmented mitochondria (Supplementary Fig. 7d), supporting CAMK2 as a selective antagonist of DRP1 function in non-BTICs (Supplementary Fig. 7e). Collectively, we propose that CDK5 activates DRP1 through phosphorylating the S616 site in BTICs while CAMK2 inhibits DRP1 activity through phosphorylation of S637 in non-BTICs, creating a competitive yoked control of metabolism within the tumor hierarchy.

Mitochondrial morphological control informs prognosis

Our findings support a model in which DRP1-mediated mitochondrial fission distinguishes BTICs. To determine the clinical relevance of these findings, we performed a combination of tissue analysis and *in silico* studies. DRP1 can be regulated at both the expression and activity levels so we performed immunohistochemistry of DRP1 using a novel tissue microarray with normal brain and glioblastoma tissues. Total DRP1 levels were similar in normal and neoplastic brain tissues but activating phosphorylation of DRP1 (DRP1^{S616}) was selectively increased in glioblastomas (Fig. 8a). The clinical significance of these findings was supported by a strong inverse correlation between phosphorylation of DRP1 (S616) and poor glioblastoma patient survival (Fig. 8b).

We then interrogated the downstream (AMPK) and upstream (CDK5 and CAMK2) regulatory nodes of DRP1 in clinical significance. Because we found that these regulators were all controlled at the expression level in BTICs, we interrogated available *in silico* glioblastoma databases. Using the large National Cancer Institute REpository for Molecular BRAin Neoplasia DaTa (REMBRANDT) glioma dataset, we found that upregulation of *AMPKα2* mRNA twofold or greater in all glioma patients (i.e. mixed-grade) correlated with a significant increase in survival (Fig. 8c). CDK5 and CAMK2 regulate DRP1 in opposite ways with high levels of CDK5 expected to associate with higher DRP1 activity and CAMK2 with lower DRP1 activity. The NCI REMBRANDT database confirmed that higher *CDK5* expression correlated with shorter patient survival (Fig. 8d) while higher *CAMK2A/2G* expression was associated with longer patient survival (Fig. 8e, 8f). Of note, mRNA gene expression signatures of putative BTIC markers (*Sox2, Olig2, Pou3/2,* and *Sall2*) are not predictive of patient survival independent of tumor grade (data not shown). Likewise, each of our targets is associated with tumor grade so lacks prognostic prediction independent of tumor grade (data not shown). A combined signature of $AMPK^{low}CDK5^{high}CAMK2^{low}$ demonstrated strong dichotomization of mixed-grade glioma patient survival (Supplementary Figure 8). These data support a clinically important role for the CDK5/CAMK2-DRP1-AMPK signaling axis in glioma.

DISCUSSION

Glioblastomas rank among the most lethal of cancers with decades of research adding only a few months to the median survival of patients afflicted with these cancers[1]. The explanation for the failure of current therapy to extend patient survival has many causes, but one contributing force may be the presence of complex intratumoral heterogeneity derived from heterogeneous expression of oncogenic drivers as well as cellular hierarchies that phenocopy the normal brain hierarchy, albeit with aberrant control (i.e. BTICs). Targeting BTICs has proven daunting because of the resistance of these cells to pathways that have served as the basis for most cancer treatments[8, 43], leading to novel discovery paradigms informed by stem cell biology. The development of anti-BTIC therapies has been largely informed by targeting core stem cell pathways described in development or tissue homeostasis. These approaches have yielded significant promise, but it is possible that aberrant control of BTICs distinct from normal neural stem cells may offer even greater benefit.

Normal neural stem cells are tightly regulated due to their ability to undergo sustained proliferation. In response, neural stem cells reside in specific niches from which their derive maintenance cues but are also constrained in proliferation and undergo differentiation upon exiting the niche. BTICs share some cell autonomous regulatory pathways with neural stem cells but also independently create elements of the neural stem niche, e.g. neovascularization. The neural stem cell niche is a structural construct but also is associated with regional variation in oxygen, pH, and nutrient availability. Thus, it is almost certain that metabolic reprogramming that occurs within the context of oncogenesis represents an element of the BTIC niche that requires control of metabolic stress responses.

Neurons express the high-affinity glucose transporter, GLUT3, which allows for these cells to outcompete their neighbors (e.g. astrocytes that express predominantly GLUT1) for

limited nutrition. We recently demonstrated that BTICs have coopted GLUT3 expression to maintain themselves in the context of limited nutrient conditions found in tumors[19]. With advances in gene expression analysis in cancer and transcriptional control of BTICs, comparative gene expression strategies have been widely used to discover novel molecular targets in cancer studies. These observations extend to BTIC discovery approaches with many targets that show elevated expression in BTICs comparison to non-BTICs[44]. We now report that BTIC control can extend beyond the scope of differentially regulated genes at the transcriptional level, like GLUT3, through a linkage to post-translational metabolic control. BTICs display preferentially fragmented mitochrondrial morphology relative to non-BTICs driven by augmented fission. The balance between mitochondrial fission and fusion is controlled by a small cohort of mediators (OPA1, MFN1, and MFN2 for fusion and DRP1 for fission)[22]. While the total protein levels of these mediators were not differentially regulated within the tumor hierarchy, DRP1 activation and localization was skewed towards the stem-like tumor cells. This functional difference was driven by an unbalanced ratio of the post-translational regulation of DRP1 phosphorylation towards activation and decreased inhibition. Our data suggests that beyond gene expression, protein modifications -- including phosphorylation, acetylation, methylation, sumoylation, and ubiquitination -- offer worthwhile avenues for further exploration in BTIC research.

Metabolism represents a domain for potential cancer therapeutic for BTICs. While IDH1 mutations promote chromatin alterations throughout a tumor to promote a loss of differentiation that can be targeted by novel small molecules, IDH1 mutations are infrequent in glioblastoma[14]. Post-mitotic neurons express CDK5, which can serve to control metabolism even in non-cycling neurons. Limited previous reports have suggested that CDK5 is expressed by glioma cell lines and may contribute to cell invasion and survival after radiation, phenotypes found in BTICs[45–47]. Thus, it appears that BTICs have coopted another neuronal metabolic control mechanism to augment cellular survival to promote tumor growth.

Aberrant metabolism is not solely a byproduct of mutations or altered transcriptional programs, but represents a driving force in the initial stages of tumorigenesis. Recently studies of BTIC metabolism in glioblastoma and leukemia have yielded disconcordant responses in relative dependence on glycolysis vs. oxidative phosphorylation and ROS levels but it is clear that the metabolic state of BTICs varies within the cellular hierarchy, like in the hierarchy of the normal hematopoietic system[17–19, 48]. As a highly specialized and dynamic organelle, the mitochondria must be central to these distinctive features in energy metabolism. We find that inhibition of DRP1-mediated mitochondrial fission decreased cellular OCR and caused metabolic stress in BTICs. In addition, we detected AMPK activation in response to such energy homeostasis, supporting energy stress. The depletion AMPK largely rescued the anti-proliferative and pro-apoptotic effects by DRP1 targeting, which is consistent with AMPK function as a tumor suppressor in BTICs[41]. Future studies may show that combining DRP1 inhibition (e.g. Mdivi-1) and AMPK activation (e.g. AICAR) may create additional synergy. As DRP1 expression and AMPK activity may be altered in response to cytotoxic ionizing radiation treatment, these therapeutic paradigms may have even greater impact when used in combination. In sum, our results implicate a close interaction between DRP1 controlled mitochondrial fission and

AMPK mediated energy stress response that awaits further detailed study of the molecular mechanism of regulation of AMPK activity by DRP1 and mitochondrial dynamics.

Our discovery of a pro-survival function of DRP1 in BTICs is particularly exciting as targeting DRP1 may increase survival of normal brain cells and improve toxicity of chemotherapy. We found that targeting DRP1 by RNA interference or a pharmacologic inhibitor retarded cell growth and induced apoptosis in BTICs with limited toxicity against normal human NPCs. In contrast with its role in BTICs, DRP1 inhibition is advancing as a target in treating several brain disorders to alleviate neuronal death in Alzheimer's, Parkinson's and Huntington's diseases[22]. For example, a recent report showed that treatment of a genetically engineered mouse model of Huntington's disease with P110-TAT, another inhibitor of DRP1, strongly reduced neurological defects[49]. Thus, systemic inhibition of DRP1 may not only directly target BTIC self-renewal and growth but also function as a protector of normal neural cells. These efforts by the neuroscience community are driving not only the development of these agents but with a focus on central nervous system delivery, permitting a potentially rapid translation into the treatment of glioblastoma and perhaps brain metastases. Our results do not rule out a loss of fusion in BTICs but targeting fission holds several distinct advantages as a therapeutic target over fusion regulators. First, to date DRP1 has been a critical mediator of fission, providing a single target rather than three targets with distinct expression and function. Secondly, DRP1 is an enzyme (GTPase) that can be inhibited with acceptable activity, especially in the brain. Finally, DRP1 inhibitors are already in early development based on benefit for neurodegenerative diseases suggesting a potential neuroprotective effect. Although the role of mitochondrial fission in neurodegeneration and other systemic toxicity caused by radiation and chemotherapy treatments has not been well investigated, it is exciting to consider that these approaches may simultaneously treat the tumor and attenuate the negative effects of conventional therapy.

METHODS

Isolation and culture of cells

Glioblastoma tissues were obtained from excess surgical materials from patients undergoing informed written consent at the Cleveland Clinic after review from a neuropathologist in accordance with an approved protocol by the Institutional Review Board. Of note, the models tested are wild type for IDH1 (data not shown). To prevent culture-induced drift, patient-derived xenografts were generated and maintained as a source of tumor cells for study. As described previously[8, 9, 19, 38, 39], cultures enriched for or depleted of BTICs were derived from primary patient brain tumor specimens or specimens passaged for seven or fewer passages as xenografts in immunocompromised mice. A Papain Dissociation System (Worthington Biochemical, Lakewood, NJ) was used to dissociate tumors according to the manufacturer's instructions (detailed protocol: http://www.worthington-biochem.com/PDS/default.html). Following dissociation, cells were cultured for at least six hours in Neurobasal media supplemented with B27 without vitamin A (Gibco, Grand Island, NY), L-glutamine, sodium pyruvate (Invitrogen, Carlsbad, CA) and 10 ng/mL each of epidermal growth factor (EGF, R&D systems, Minneapolis, MN) and basic fibroblast growth factor (bFGF, R&D

systems) for surface antigen recovery. To investigate mitochondrial control in BTICs, we isolated functionally validated matched BTIC and non-BTIC populations from patient xenografts using the BTIC marker, CD133 or CD15 (SSEA1). As noted above, the derivation of BTICs requires functional validation. Where indicated, BTICs and non-BTICs were derived immediately after dissociation or after transient, low passage as xenografts in immunocompromised mice using prospective sorting followed by assays to confirm stem cell marker expression, sphere formation, and secondary tumor initiation. In the models used in these studies, CD133 has previously identified functional BTICs. While CD133 has been controversial as a BTIC marker because it has not been universally informative across all tumors and is not likely exclusively expressed by BTICs, we have found in most models tested that acute use of CD133 from an in vivo environment can segregate BTICs and non-BTICs. Therefore, in experiments with matched BTIC or non-BTIC cultures we segregated CD133 marker-positive and marker-negative populations using CD133/2-APC conjugated antibody (293C3, Miltenyi Biotech, Auburn, CA) by FACS or magnetic bead separation (Miltenyi), as previously described[8, 9, 19, 38, 39]. The BTIC phenotype of these cells was validated by stem cell marker expression (CD133, Olig2, Sox2), functional assays of self-renewal (serial tumorsphere passage), and tumor propagation such as in vivo limiting dilution assays. Human Neural Progenitor Cells (NPCs) were derived from fetal brains (15167, Lonza, Allendale, NJ) or from directed differentiation of embryonic stem cells (ENSA, Millipore, Billerica, MA) then cultured and maintained in suspension culture according to vendor's instructions or propagated on the BD stem cell Matrigel-coated dishes (BD Biosystems, San Jose, CA) using Neurobasal stem cell media as indicated. All tumor models were cultured under identical, serum-free conditions during experiments, except for studies of induced differentiation of BTICs (Figure 2E), which involved culture in DMEM with 10% serum.

Immunofluorescent staining

Cells or 10 μm thick slices of xenografted brain tissue were fixed in 4% paraformaldehyde and immunolabeled using the following antibodies: DRP1 (BD Biosystems), phospho-DRP1^{S616} (Cell Signaling, Danvers, MA), TOM20 (Santa Cruz Biotechnology, Santa Cruz, CA), OLIG2 (R&D Systems), and SOX2 (R&D Systems). Primary antibodies were incubated overnight at 4°C, followed by species appropriate secondary antibodies (Alexa 488 and 568; Invitrogen Molecular Probes, Eugene, OR) with incubation for 1 hour. Nuclei were stained with DAPI, and slides were then mounted using Fluoromount (Calbiochem, San Diego, CA). Images were taken using a Leica Titan confocal or DM4000 Upright microscopy.

Vectors and lentiviral transfection

Lentiviral clones to express either shRNA directed against Drp1 (TRCN0000001097, TRCN0000318425), CDK1 (TRCN0000196602, TRCN0000000583, TRCN0000196603), CDK5 (TRCN0000195513, TRCN0000194974, TRCN0000199652) or a non-targeting (NT) shRNA (SHC002) were obtained from Sigma-Aldrich (St. Louis, MO). The NT vector contains an shRNA insert that does not target human or mouse genes, serving as a negative control for off-target effects in experiments. Lentiviral shRNA clone targeting AMPKα (sc-45132-SH) and a scrambled non-targeting control (sc-108060) were purchased from

Santa Cruz Biotechnology. shRNAs with non-overlapping sequences that had the best relative knockdown efficiency were used for all experiments. Lentiviral particles were generated in 293FT cells in stem cell media with co-transfection with the packaging vectors pCMV-dR8.2 dvpr and pCI-VSVG (Addgene) by Lipofectamine 2000 (Invitrogen). Efficiency of lentiviral shRNA clones was determined by immunoblot and real-time PCR. Viral stocks were concentrated via precipitation using the PEG-8000, and then subsequently titered using the manufacturer's protocol. A $Drp1^{S616E/S637A}$ mutant was generated by QuickChange Multi III Site-Directed Mutagenesis kit (Stratagene, North Torrey Pines, CA) and confirmed by sequencing. Sequences for primer sets were as follows: $Drp1^{S616E}$ Forward: ATTCCAATTATGCCAGCCGAGCCACAAAAAGGTCATGCCGT; $Drp1^{S616E}$ Reverse: ACGGCATGACCTTTTTGTGGCTCGGCTGGCATAATTGGAAT; $Drp1^{S637A}$ Forward: GTTCCTGTTGCACGAAAACTAGCTGCTCGGGAAC; $Drp1^{S637A}$ Reverse: GTTCCCGAGCAGCTAGTTTTCGTGCAACAGGAAC.

Quantitative RT-PCR

Total cellular RNA was isolated using the RNeasy kit (Qiagen, Venlo, Netherlands) and reverse transcribed into cDNA using qScriptcDNASuperMix (Quanta Biosciences, Gaithersburg, MD). mRNA levels were measured using an ABI-7900 system (Applied Biosystems, Carlsbad, CA). Quantitative reverse transcription PCR was performed per the manufacturer's protocol on an Applied Biosystems 7900HT cycler using SYBR Green Master mix (SA Biosciences, Valencia, CA) and gene-specific primers.

Western Blotting

Cells were collected and lysed in hypotonic buffer with nonionic detergent (50 mM Tris-HCl, pH 7.5; 150 mM NaCl; 0.5% NP-40, 50 mM NaF with protease inhibitors), incubated on ice for 15 minutes and cleared by centrifugation at 10,000 g at 4°C for 10 minutes. Protein concentration was determined using the Bradford assay (Bio-Rad Laboratories, Hercules, CA). Equal amounts of protein (10 μg) were mixed with reducing Laemmli loading buffer, boiled and electrophoresed on NuPAGE Gels (Invitrogen), then transferred to PVDF membranes (Millipore). Blocking was performed for 30 minutes with 5% nonfat dry milk in TBST and blotting performed with primary antibodies at 1:1000 dilution (except TUBULIN (1:5000) and OLIG2 (1:500)) for 16 hours at 4°C. Antibodies included DRP1 (BD, 611738), phospho-$DRP1^{S616}$ (Cell Signaling, CST-4494), phospho-$DRP1^{S637}$ (Cell Signaling, CST-6319), CD133/1 (Miltenyi, 120-000-312), SOX2 (Santa Cruz Biotechnology, sc-17320), OLIG2 (R&D Systems, AF2418), GFAP (Covance, Princeton, NJ, PRB-571), TOM20 (Santa Cruz Biotechnology, sc-11415), PARP (Cell Signaling, CST-9532), CDK1 (Cell Signaling, CST-9116), CDK5 (Santa Cruz Biotechnology, sc-6247), CAMK1 (Santa Cruz Biotechnology, sc-33165), CAMK2 (Abcam, ab22609), MFN1 (Santa Cruz Biotechnology, sc-50330), MFN2 (Abcam, Cambridge, MA, ab56889), OPA1 (Abcam, ab42364), AMPKα (Cell Signaling, CST-5831), phospho-AMPKαT172 (Cell Signaling, CST-4188), TUBULIN(Sigma, T9026) and GAPDH (Sigma, SAB1405848; and Cell Signaling, CST-2218).

Proliferation and Neurosphere Formation assay

Cell proliferation assay using Cell-Titer Glow (Promega, Madison, WI) and neurosphere formation were measured as per the manufacturer's protocol as previously described (8, 9, 19, 38, 39). All data were normalized to day 0 and presented as mean ± standard error.

Electron microscopy

Matched BTICs and non-BTICs were fixed in 2.5% glutaraldehyde-4% paraformaldehyde in 0.1 M cacodylate buffer, overnight at 4°C. This was followed by post-fixation with 1% osmium tetraoxide for 1 hour. Samples were washed and following by staining with 1% uranyl acetate in Maleate buffer. After ethanol dehydration, samples were embedded with eponate 12 medium. Sections (85 nm) were cut using a diamond knife, stained with uranyl acetate and lead citrate, and then observed with a Tecnai G2 SpiritBT electron microscope operated at 60 kV.

Mitochondria Isolation

Mitochondria were isolated using Mitochondria Isolation Kit (89874, Pierce, Rockford, IL), according to the manufacturer's instructions.

Measurement of oxygen consumption rate (OCR)

Oxygen consumption rate (OCR) was determined using the Seahorse XF Extracellular Flux Analyzer (Seahorse Bioscience, North Billerica, MA). BTICs were plated at 80,000 cells per well for measurement. Three metabolic inhibitors were sequentially loaded to each well at specific time points: Oligomycin (0.75 μM), followed by FCCP (0.75 μM), followed by the addition of a combination of Rotenone (0.1 μM) and Antimycin (0.1 μM).

In vitro limiting dilution assay

For in vitro limiting dilution assays, cells were sorted by fluorescence-activated cell sorting (FACS) with decreasing numbers of cells per well (20, 10, 5, and 1) plated in 96-well plates. Ten days after plating, the presence and number of neurospheres in each well was quantified. Extreme limiting dilution analysis was performed using software available at http://bioinf.wehi.edu.au/software/elda, as previously described[8, 9, 19, 38, 39].

Intracranial tumor formation in vivo

GICs were transduced with lentiviral vectors expressing Drp1 or a non-targeting (NT) control shNRA for the knockdown experiments. 36 hours post infection, viable cells were counted and engrafted intracranially into NS, (NOD.Cg-PrkdBTICid Il2rgtm1Wjl/SzJ) mice under a Cleveland Clinic Foundation Institutional Animal Care and Use Committee approved protocol. Animals were then maintained until neurological signs were apparent, at which point they were sacrificed. The brains were harvested and fixed in 4% formaldehyde, cryopreserved in 30% sucrose, and then cryosectioned. Sections were stained with hematoxylin and eosin. In parallel survival experiments, animals were monitored until they developed neurological signs.

Immunohistochemical quantification of glioma tissue microarrays (TMAs)

Expression of total DRP1 and phosphorylated DRP1^{S616} in WHO grades II-IV gliomas was performed on TMAs similar to that previously described[50]. Briefly, a TMA of deidentified formalin-fixed, paraffin-embedded (FFPE) gliomas was immunonstained for DRP1 (1:100, BD Transduction Laboratories, San Jose, CA) or phospho-DRP1^{S616} (1:200, Cell Signaling, Danvers, MA). Secondary antibodies used were EnVision labeled polymer-HRP (horseradish peroxidase) anti-mouse or anti-rabbit as appropriate. Staining was visualized using 3, 3′-diaminobenzidine (DAB) chromogen (Dako, Carpinteria, CA). Each tumor was represented by three separate 2 mm cores on the TMA, with each core embedded in a separate TMA block. Each TMA core was semiquantified on a relative scale of intensity from 0 to 3, with 0 = negative and 3 = strongest. Results from all three cores were averaged together to produce a final score for a tumor. For survival analysis, ratios of phosphorylated-to-total DRP1 were calculated for each tumor (represented by three cores each) and a mean score was derived across all tumors. Dichotomized levels (high vs. low) were assigned relative to the global mean value. Each case was annotated with clinical data from the Kentucky Cancer Registry.

Bioinformatic analysis

National Cancer Institute's Repository for Molecular Brain Neoplasia Data (REMBRANDT, https://caintegrator.nci.nih.gov/rembrandt/) or The Cancer Genome Atlas (TCGA, https://tcga-data.nci.nih.gov/tcga/tcgaHome2.jsp) microarray databases annotated with patient survival were used to correlate survival and multiple gene expression in malignant glioma biopsies.

Statistical analysis

No statistical methods were used to pre-determine sample sizes but our sample sizes are similar to those reported in previous publications[8, 9, 19, 38, 39]. Data acquisition and analysis was not blinded. All grouped data are presented as mean ± standard error of the mean (s.e.m.). Data distribution was assumed to be normal but this was not formally tested. Differences between groups were assessed by Student's t-test or ANOVA using GraphPadInStat software (GraphPad Software, La Jolla, CA). Kaplan-Meier curves were generated and log-rank analysis was performed using MedCalc software (Ostend, Belgium). A supplementary methods checklist is available.

Supplementary Material

Refer to Web version on PubMed Central for supplementary material.

ACKNOWLEDGMENTS

We appreciate flow cytometry assistance from C. Shemo and S. O'Bryant, and the tissue provided by Mary McGraw, the Cleveland Clinic Foundation Tissue Procurement Service and A. E. Sloan (University Hospitals). Ichiro Nakano (Ohio State University) kindly provided the IN528 model. We would like to thank members of the Rich laboratory for critical reading of the manuscript and helpful discussions. We would like to thank A. Janocha for help with using the Seahorse XF Extracellular Flux Analyzer. Finally, we would like to thank our funding sources: The National Institutes of Health grants CA154130, CA169117, CA171652, NS087913, NS089272 (J.N.R), CA155764, 2P20 RR020171 COBRE pilot grant (C.M.H.) and NS070315 (S.B.), Research Programs Committees of Cleveland Clinic (J.N.R), and James S. McDonnell Foundation (J.N.R). C.M.H. was supported by

The Peter and Carmen Lucia Buck Training Program in Translational Clinical Oncology, and the University of Kentucky College of Medicine Physician Scientist Program. The Markey Biospecimen and Tissue Procurement (BSTP) Shared Resource Facility facilitated the construction of tissue microarrays and immunohistochemical studies. The BSTP Shared Resource Facility is supported by the University of Kentucky Markey Cancer Center (P30CA177558). Special thanks to Dana Napier for her excellent histologic expertise.

REFERENCES

1. Stupp R, et al. Effects of radiotherapy with concomitant and adjuvant temozolomide versus radiotherapy alone on survival in glioblastoma in a randomised phase III study: 5-year analysis of the EORTC-NCIC trial. The lancet oncology. 2009; 10:459–466. [PubMed: 19269895]
2. Brennan CW, et al. The somatic genomic landscape of glioblastoma. Cell. 2013; 155:462–477. [PubMed: 24120142]
3. Frattini V, et al. The integrated landscape of driver genomic alterations in glioblastoma. Nature genetics. 2013; 45:1141–1149. [PubMed: 23917401]
4. Singh SK, et al. Identification of human brain tumour initiating cells. Nature. 2004; 432:396–401. [PubMed: 15549107]
5. Galli R, et al. Isolation and characterization of tumorigenic, stem-like neural precursors from human glioblastoma. Cancer research. 2004; 64:7011–7021. [PubMed: 15466194]
6. Hemmati HD, et al. Cancerous stem cells can arise from pediatric brain tumors. Proceedings of the National Academy of Sciences of the United States of America. 2003; 100:15178–15183. [PubMed: 14645703]
7. Gage FH, Temple S. Neural stem cells: generating and regenerating the brain. Neuron. 2013; 80:588–601. [PubMed: 24183012]
8. Bao S, et al. Glioma stem cells promote radioresistance by preferential activation of the DNA damage response. Nature. 2006; 444:756–760. [PubMed: 17051156]
9. Bao S, et al. Stem cell-like glioma cells promote tumor angiogenesis through vascular endothelial growth factor. Cancer research. 2006; 66:7843–7848. [PubMed: 16912155]
10. Gunther HS, et al. Glioblastoma-derived stem cell-enriched cultures form distinct subgroups according to molecular and phenotypic criteria. Oncogene. 2008; 27:2897–2909. [PubMed: 18037961]
11. Sarkar S, et al. Therapeutic activation of macrophages and microglia to suppress brain tumor-initiating cells. Nature neuroscience. 2014; 17:46–55. [PubMed: 24316889]
12. Zhou BB, et al. Tumour-initiating cells: challenges and opportunities for anticancer drug discovery. Nature reviews. Drug discovery. 2009; 8:806–823. [PubMed: 19794444]
13. Ward PS, Thompson CB. Metabolic reprogramming: a cancer hallmark even warburg did not anticipate. Cancer cell. 2012; 21:297–308. [PubMed: 22439925]
14. Yan H, et al. IDH1 and IDH2 mutations in gliomas. The New England journal of medicine. 2009; 360:765–773. [PubMed: 19228619]
15. Turcan S, et al. IDH1 mutation is sufficient to establish the glioma hypermethylator phenotype. Nature. 2012; 483:479–483. [PubMed: 22343889]
16. Marin-Valencia I, et al. Analysis of tumor metabolism reveals mitochondrial glucose oxidation in genetically diverse human glioblastomas in the mouse brain in vivo. Cell metabolism. 2012; 15:827–837. [PubMed: 22682223]
17. Vlashi E, et al. Metabolic state of glioma stem cells and nontumorigenic cells. Proceedings of the National Academy of Sciences of the United States of America. 2011; 108:16062–16067. [PubMed: 21900605]
18. Kathagen A, et al. Hypoxia and oxygenation induce a metabolic switch between pentose phosphate pathway and glycolysis in glioma stem-like cells. Acta neuropathologica. 2013; 126:763–780. [PubMed: 24005892]
19. Flavahan WA, et al. Brain tumor initiating cells adapt to restricted nutrition through preferential glucose uptake. Nature neuroscience. 2013; 16:1373–1382. [PubMed: 23995067]
20. Janiszewska M, et al. Imp2 controls oxidative phosphorylation and is crucial for preserving glioblastoma cancer stem cells. Genes & development. 2012; 26:1926–1944. [PubMed: 22899010]

21. Ochocki JD, Simon MC. Nutrient-sensing pathways and metabolic regulation in stem cells. The Journal of cell biology. 2013; 203:23–33. [PubMed: 24127214]
22. Archer SL. Mitochondrial dynamics--mitochondrial fission and fusion in human diseases. The New England journal of medicine. 2013; 369:2236–2251. [PubMed: 24304053]
23. Chen H, et al. Mitofusins Mfn1 and Mfn2 coordinately regulate mitochondrial fusion and are essential for embryonic development. The Journal of cell biology. 2003; 160:189–200. [PubMed: 12527753]
24. Todd LR, Gomathinayagam R, Sankar U. A novel Gfer-Drp1 link in preserving mitochondrial dynamics and function in pluripotent stem cells. Autophagy. 2010; 6:821–822. [PubMed: 20581476]
25. Todd LR, et al. Growth factor erv1-like modulates Drp1 to preserve mitochondrial dynamics and function in mouse embryonic stem cells. Molecular biology of the cell. 2010; 21:1225–1236. [PubMed: 20147447]
26. Kashatus DF, et al. RALA and RALBP1 regulate mitochondrial fission at mitosis. Nature cell biology. 2011; 13:1108–1115. [PubMed: 21822277]
27. Zhao J, et al. Mitochondrial dynamics regulates migration and invasion of breast cancer cells. Oncogene. 2013; 32:4814–4824. [PubMed: 23128392]
28. Thomas KJ, Jacobson MR. Defects in mitochondrial fission protein dynamin-related protein 1 are linked to apoptotic resistance and autophagy in a lung cancer model. PloS one. 2012; 7:e45319. [PubMed: 23028930]
29. Guido C, et al. Mitochondrial fission induces glycolytic reprogramming in cancer-associated myofibroblasts, driving stromal lactate production, and early tumor growth. Oncotarget. 2012; 3:798–810. [PubMed: 22878233]
30. Palorini R, et al. Oncogenic K-ras expression is associated with derangement of the cAMP/PKA pathway and forskolin-reversible alterations of mitochondrial dynamics and respiration. Oncogene. 2013; 32:352–362. [PubMed: 22410778]
31. Rehman J, et al. Inhibition of mitochondrial fission prevents cell cycle progression in lung cancer. FASEB journal : official publication of the Federation of American Societies for Experimental Biology. 2012; 26:2175–2186. [PubMed: 22321727]
32. Wan YY, et al. Involvement of Drp1 in hypoxia-induced migration of human glioblastoma U251 cells. Oncology reports. 2014
33. Taguchi N, Ishihara N, Jofuku A, Oka T, Mihara K. Mitotic phosphorylation of dynamin-related GTPase Drp1 participates in mitochondrial fission. The Journal of biological chemistry. 2007; 282:11521–11529. [PubMed: 17301055]
34. Cribbs JT, Strack S. Reversible phosphorylation of Drp1 by cyclic AMP-dependent protein kinase and calcineurin regulates mitochondrial fission and cell death. EMBO reports. 2007; 8:939–944. [PubMed: 17721437]
35. Kasahara A, Cipolat S, Chen Y, Dorn GW 2nd, Scorrano L. Mitochondrial fusion directs cardiomyocyte differentiation via calcineurin and Notch signaling. Science. 2013; 342:734–737. [PubMed: 24091702]
36. Tanaka A, Youle RJ. A chemical inhibitor of DRP1 uncouples mitochondrial fission and apoptosis. Molecular cell. 2008; 29:409–410. [PubMed: 18313377]
37. Gharanei M, Hussain A, Janneh O, Maddock H. Attenuation of doxorubicin-induced cardiotoxicity by mdivi-1: a mitochondrial division/mitophagy inhibitor. PloS one. 2013; 8:e77713. [PubMed: 24147064]
38. Eyler CE, et al. Glioma stem cell proliferation and tumor growth are promoted by nitric oxide synthase-2. Cell. 2011; 146:53–66. [PubMed: 21729780]
39. Cheng L, et al. Glioblastoma stem cells generate vascular pericytes to support vessel function and tumor growth. Cell. 2013; 153:139–152. [PubMed: 23540695]
40. Son MJ, Woolard K, Nam DH, Lee J, Fine HA. SSEA-1 is an enrichment marker for tumor-initiating cells in human glioblastoma. Cell stem cell. 2009; 4:440–452. [PubMed: 19427293]
41. Sato A, et al. Glioma-initiating cell elimination by metformin activation of FOXO3 via AMPK. Stem cells translational medicine. 2012; 1:811–824. [PubMed: 23197693]

42. Han XJ, et al. CaM kinase I alpha-induced phosphorylation of Drp1 regulates mitochondrial morphology. The Journal of cell biology. 2008; 182:573–585. [PubMed: 18695047]
43. Eramo A, et al. Chemotherapy resistance of glioblastoma stem cells. Cell death and differentiation. 2006; 13:1238–1241. [PubMed: 16456578]
44. Anido J, et al. TGF-beta Receptor Inhibitors Target the CD44(high)/Id1(high) Glioma-Initiating Cell Population in Human Glioblastoma. Cancer cell. 2010; 18:655–668. [PubMed: 21156287]
45. Catania A, et al. Expression and localization of cyclin-dependent kinase 5 in apoptotic human glioma cells. Neuro-oncology. 2001; 3:89–98. [PubMed: 11296485]
46. Gao C, et al. Cdk5 mediates changes in morphology and promotes apoptosis of astrocytoma cells in response to heat shock. Journal of cell science. 2001; 114:1145–1153. [PubMed: 11228158]
47. Liu R, et al. Cdk5-mediated regulation of the PIKE-A-Akt pathway and glioblastoma cell invasion. Proceedings of the National Academy of Sciences of the United States of America. 2008; 105:7570–7575. [PubMed: 18487454]
48. Lagadinou ED, et al. BCL-2 inhibition targets oxidative phosphorylation and selectively eradicates quiescent human leukemia stem cells. Cell stem cell. 2013; 12:329–341. [PubMed: 23333149]
49. Guo X, et al. Inhibition of mitochondrial fragmentation diminishes Huntington's disease-associated neurodegeneration. The Journal of clinical investigation. 2013; 123:5371–5388. [PubMed: 24231356]
50. Gilbert MR, et al. Autophagy and oxidative stress in gliomas with IDH1 mutations. Acta neuropathologica. 2014; 127:221–233. [PubMed: 24150401]

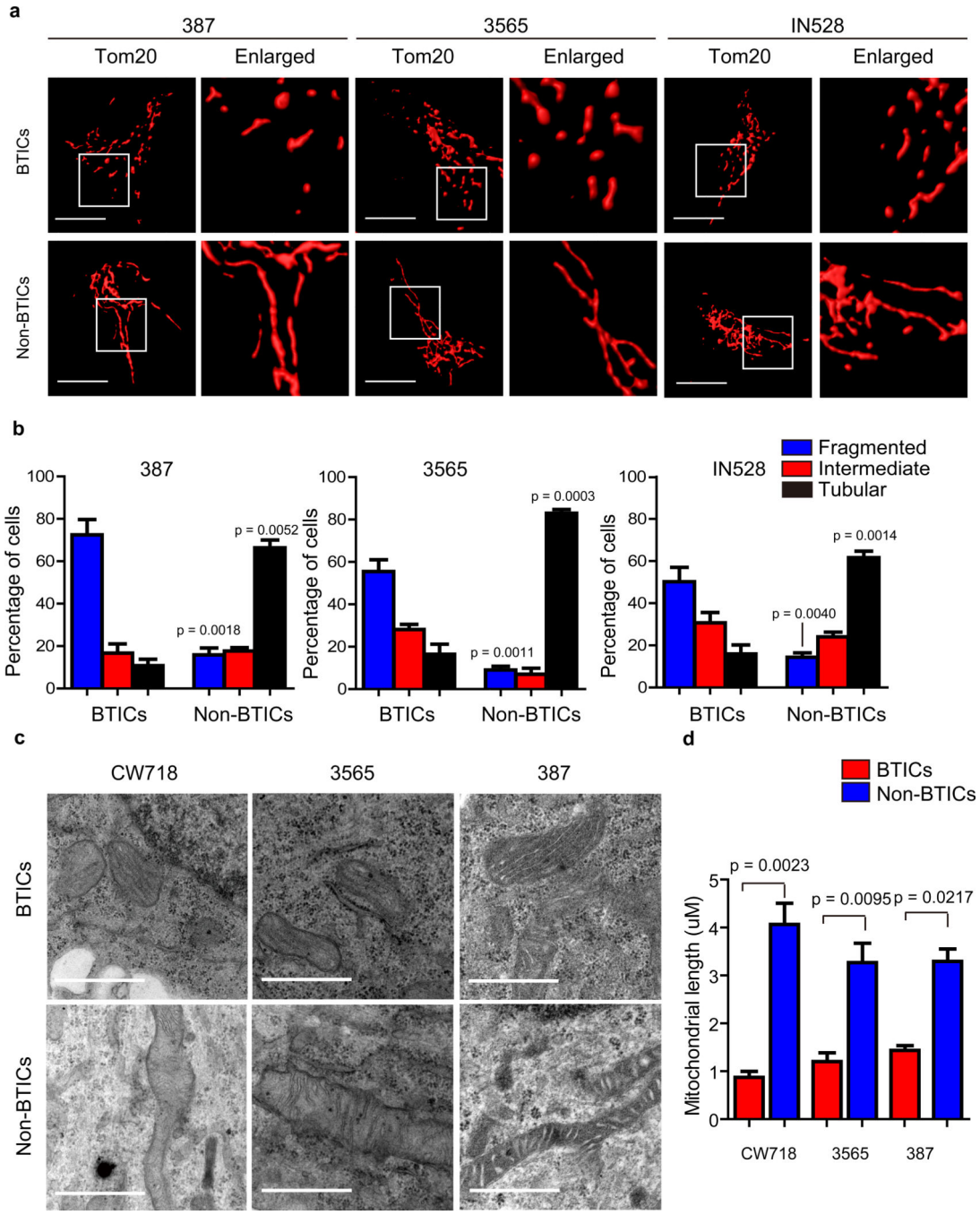

Figure 1. Brain tumor initiating cells and non-brain tumor initiating cells display distinct mitochondrial morphologies

a. Mitochondria of brain tumor initiating cells (BTICs) and non-BTICs isolated from patient-derived xenografts (387, 3565, and IN528) were visualized with anti-TOM20 antibody. Scale bars, 5μm. **b**. Mitochondria morphology was assessed from 150 cells of three different slides. Data are presented as mean ± s.e.m. (387, fragmented: p = 0.0018, tubular: p = 0.0052; 3565, fragmented: p = 0.0011, tubular: p = 0.0003; IN528, fragmented: p = 0.0040, tubular: p = 0.0014; statistical significance determined by Student's t-test; n =

3). **c**. Transmission electron microscopy images of mitochondria in glioblastoma BTICs and non-BTICs isolated from three xenografts (CW718, 3565, and 387). At least 30 mitochondria were analyzed per experiment. Scale bars, 1 μm. Data are presented as mean ± s.e.m. (CW718, p = 0.0023; 3565, p = 0.0095; 387, p = 0.0217; statistical significance determined by Student's t-test; n = 3).

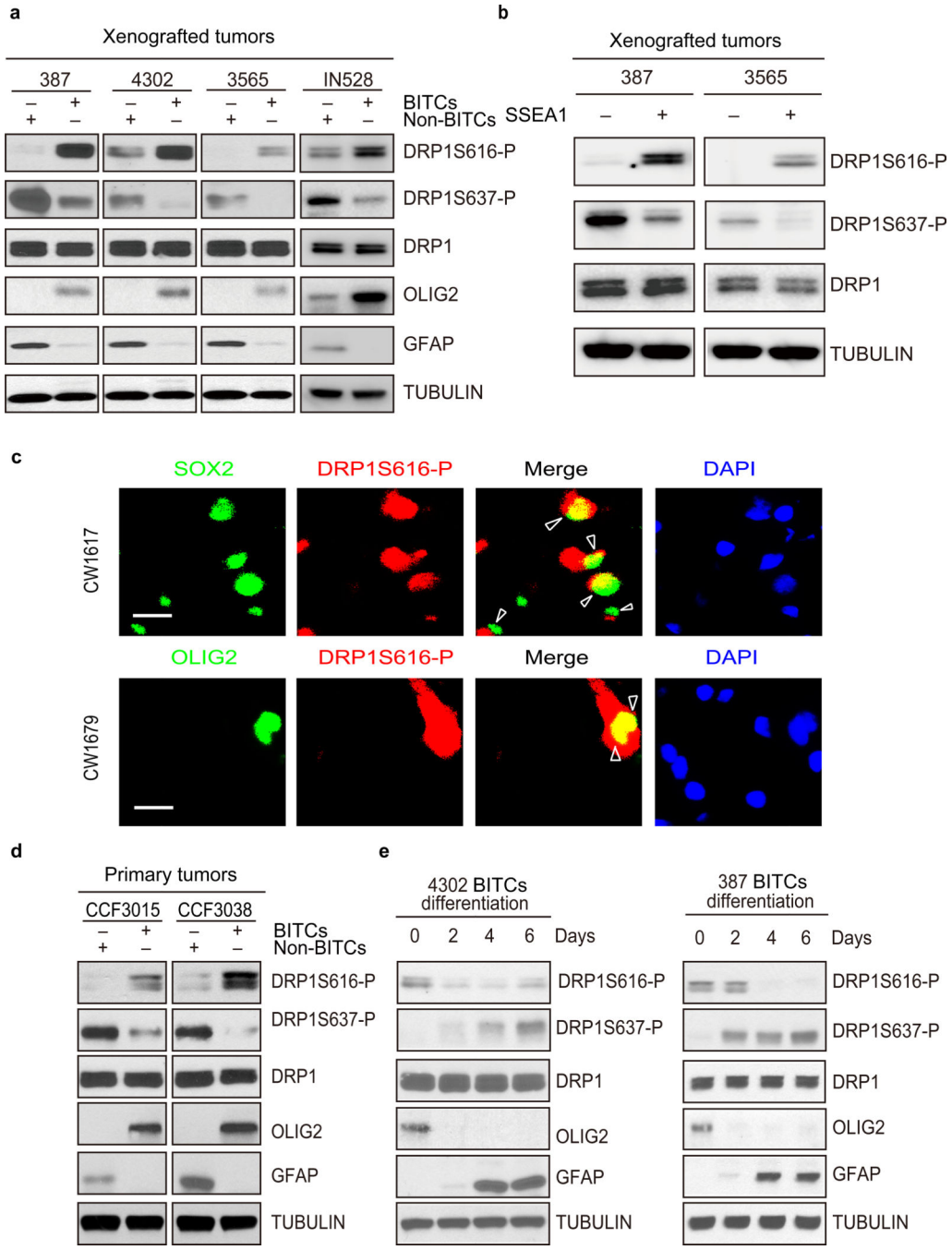

Figure 2. DRP1 is hyperactivated in brain tumor initiating cells

a. Immunoblot analysis of DRP1 total protein levels and activating phosphorylation [phospho-DRP1^{S616}] and repressive phosphorylation [phospho-DRP1^{S637}] in BTICs and non-BTICs isolated from patient-derived xenografts (T387, T4302, T3565, and IN528). Images were cropped for presentation. Full-length blots are presented in Supplementary Fig. 9. **b**. Alternative enrichment of BTICs from patient-derived xenografts (387 and 3565) by SSEA1/CD15 confirmed differential activation on immunoblot of phospho-DRP1. **c**. Immunofluorescent staining of activating phosphorylation of DRP1 [phospho-DRP1^{S616}]

with several BTIC markers, including SOX2 and OLIG2 in two primary human GBM specimens (CW1617, CW1679). **d**. Immunoblot analysis of DRP1 protein and its activating phosphorylation [phospho-DRP1^{S616}] and repressive phosphorylation [phopho-DRP1^{S637}] in BTICs and non-BTICs directly derived from two primary human glioblastoma specimens (CCF3015 and CCF3038). **e**. Immunoblot analysis of phospho-DRP1^{S616} and phospho-DRP1^{S637} levels during BTIC (4302 and 387) differentiation induced by 10% serum over a time course.

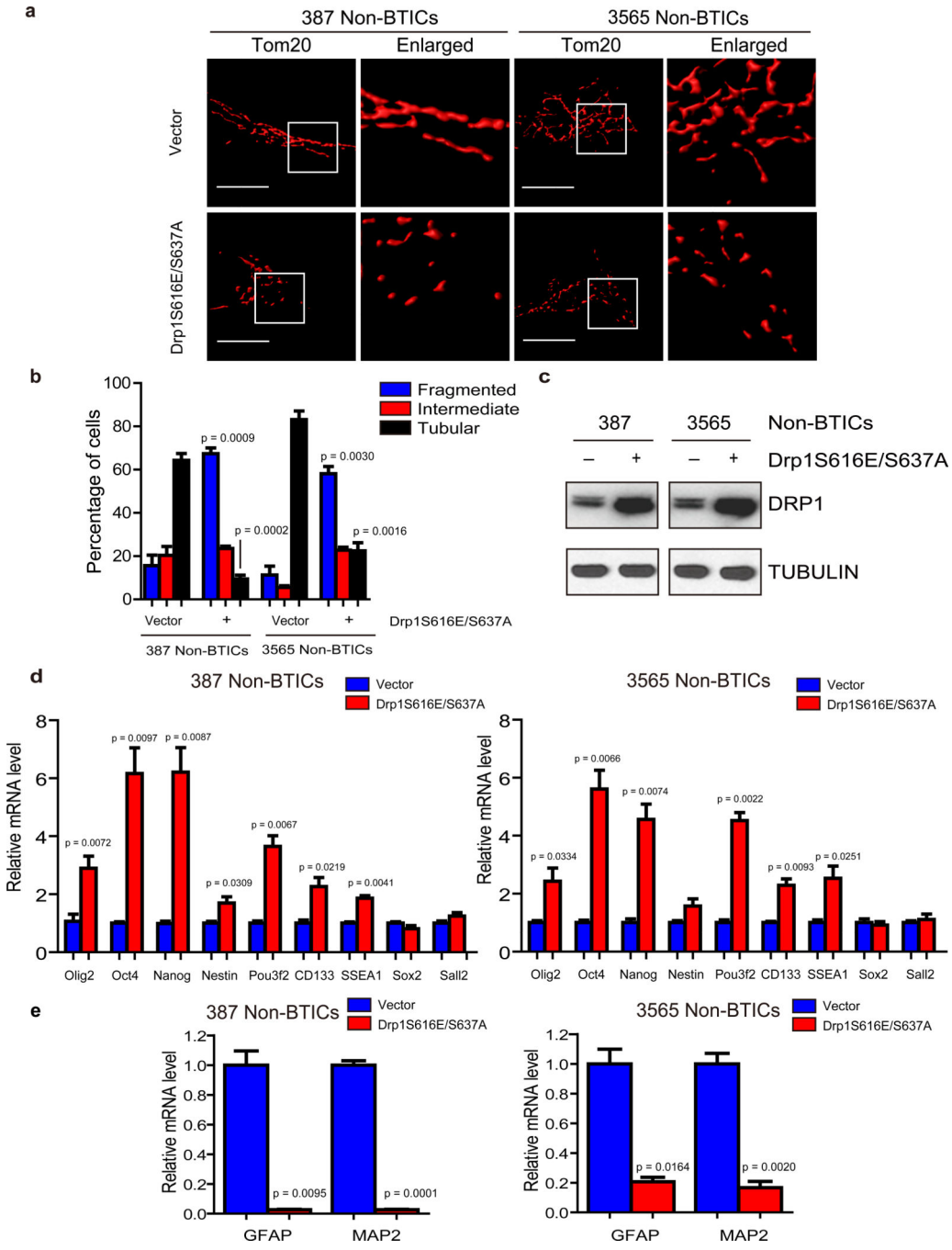

Figure 3. DRP1 phosphorylation regulates mitochondrial morphology and stem cell marker expression

a. Immunofluorescent staining of mitochondria by TOM20 in 387 and 3565 non-brain tumor initiating cells (non-BTICs) transduced by lentiviral control vector or a DRP1$^{S616E/S637A}$ double mutant. **b**. Mitochondria morphology was assessed from 120 cells of three different experiments. Data are displayed as mean ± s.e.m. (387, fragmented: p = 0.0009, tubular: p = 0.0002; 3565, fragmented: p = 0.0030, tubular: p = 0.0016; statistical significance determined by Student's t-test; n = 3). **c**. Immunoblot analysis of DRP1 protein in 387 and

3565 non-BTICs expressing control vector or a DRP1$^{S616E/S637A}$ double mutant. Images were cropped for presentation. Full-length blots are presented in Supplementary Fig. 10. **d, e**. 387 non-BTICs were transduced with vector encoding a DRP1$^{S616E/S637A}$ double mutant or control vector. Three days after infection, total RNA was isolated and cDNA was synthesized by reverse transcription. The mRNA levels of indicated genes were detected by real-time qPCR. Data are displayed as mean ± s.e.m. (387: *Olig2*, p = 0.0072; *Oct4*, p = 0.0097; *Nanog*, p = 0.0087; *Nestin*, p= 0.0309; *Pou3f2*, p= 0.0067; *CD133*, p = 0.0219; *SSEA1*, p = 0.0041; *GFAP*, p = 0.0095; *MAP2*, p = 0.0001. 3565: *Olig2*, p = 0.0334; *Oct4*, p = 0.0097; *Nanog*, p = 0.0074; *Pou3f2*, p = 0.0022; *CD133*, p = 0.0093; *SSEA1*, p = 0.0251; *GFAP*, p = 0.0164; *MAP2*, p = 0.0020. Statistical significance determined by Student's t-test; n = 3).

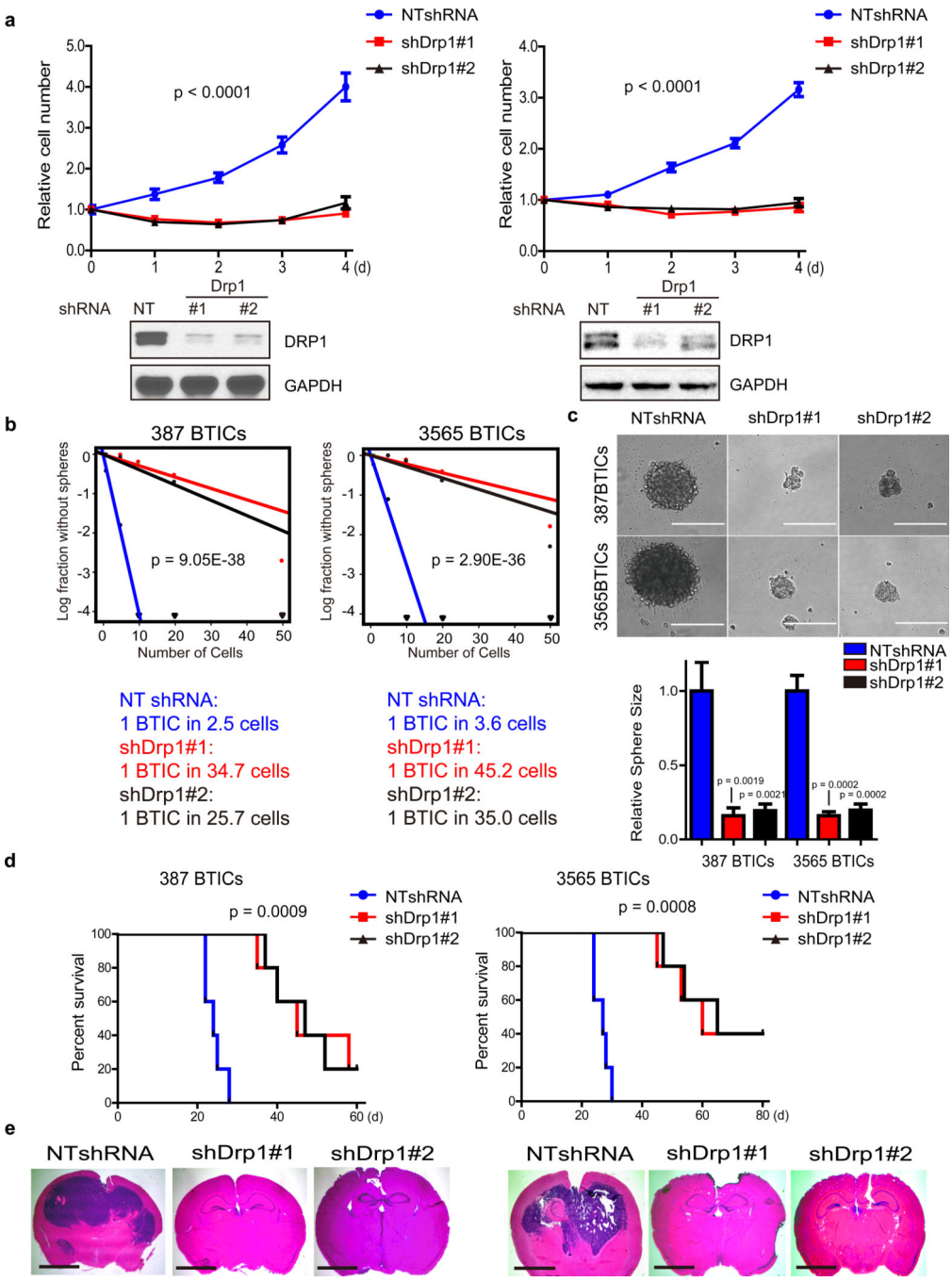

Figure 4. Targeting DRP1 by RNA interference decreases brain tumor initiating cell growth, self-renewal, and tumor formation capacity

a. Top: Effects of *Drp1* knockdown with two independent lentiviral shRNA constructs on cell proliferation in two brain tumor initiating cell (BTIC) models (387 and 3565). Data are displayed as mean ± s.e.m. ($p < 0.0001$ for both models; statistical significance determined by repeated measures ANOVA; n = 3). Bottom: Immunoblot of DRP1 following knockdown via shRNAs compared to non-targeting control shRNA sequence (NT shRNA) in two BTIC models. Images were cropped for presentation. Full-length blots are presented in

Supplementary Fig. 10. **b**. In vitro extreme limiting dilution assays (ELDA) to single cells demonstrate that knockdown of DRP1 in two BTIC models (387 and 3565) decreases the frequency of tumorsphere formation (387, $p = 9.05 \times 10^{-38}$; 3565, $p= 2.9 \times 10^{-36}$ by ANOVA). **c**. Representative images of tumorspheres derived from BTICs (387 and 3565) expressing NT control shRNA, shDrp1#1, or shDrp1#2 are shown. Scale bars, 100 μm. Quantification shows reduced tumorsphere size with DRP1 knockdown (387: shDrp1#1, p = 0.0019; shDrp1#2, p = 0.0021. 3565: shDrp1#1, p = 0.0002; shDrp1#2, p = 0.0002. ANOVA, n = 3). **d**. Kaplan-Meier survival curves of immunocompromised mice bearing orthotopic BTICs (387 and 3565) expressing NT control shRNA, shDrp1#1, or shDrp1#2 (387, p = 0.0009; 3565, p = 0.0008 by log-rank analysis; n = 5). **e**. Representative images of cross sections (hematoxylin and eosin [H&E] stained) of mouse brains harvested on day 24 (left: 3565 BTICs) or day 22 (right: 387 BTICs) after transplantation of BTICs expressing NT control shRNA, shDrp1#1, or shDrp1#2. Scale bars, 2 mm.

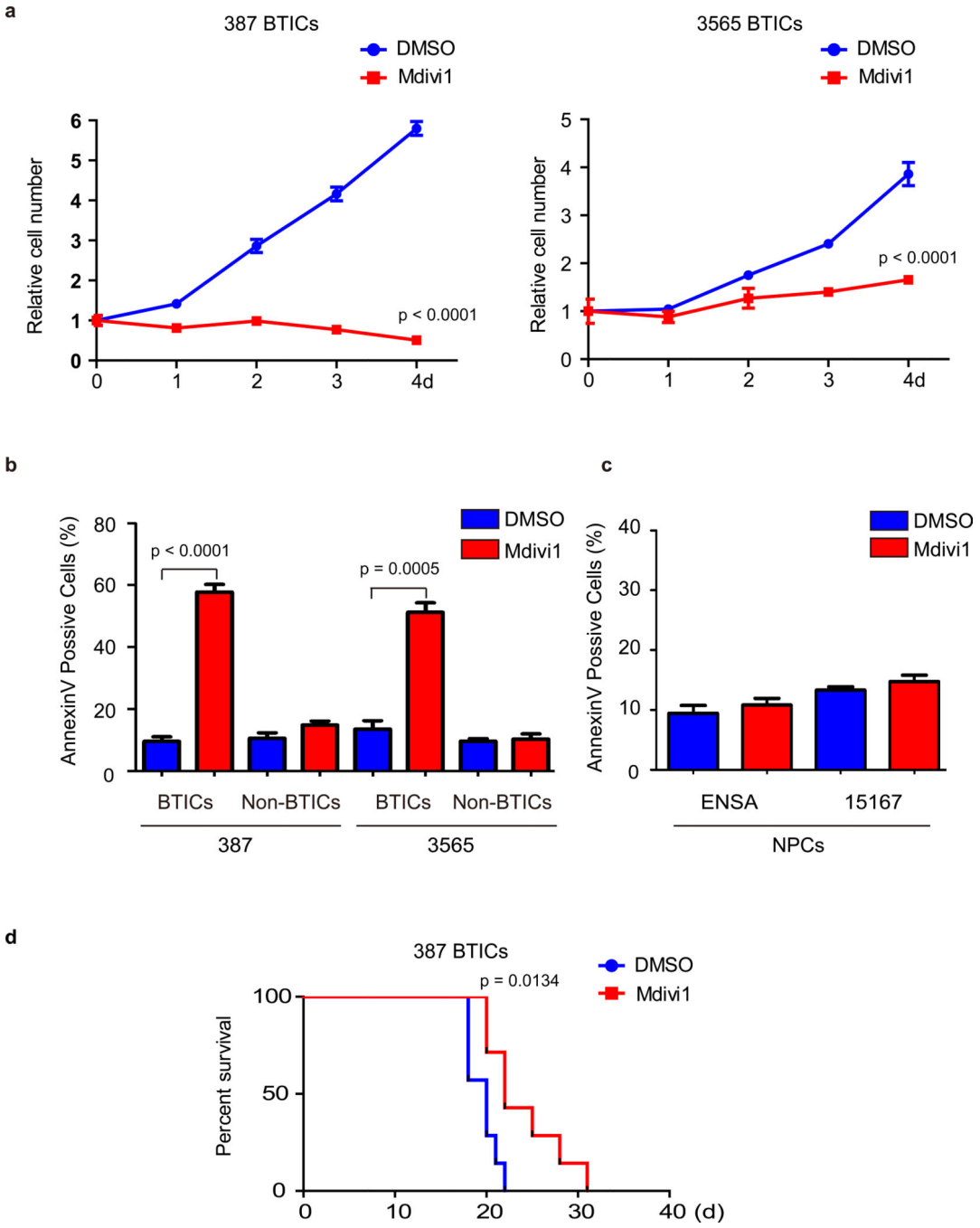

Figure 5. DRP1 inhibitor Mdivi-1 reduces brain tumor initiating cell growth and induces apoptosis

a. Effects of Mdivi-1 treatment on cell proliferation in two brain tumor initiating cell (BTIC) models (387 and 3565). Plotted data are mean ± s.e.m. (387: 4 d, $p < 0.0001$; 3565: 4d, $p < 0.0001$; $n = 4$). **b**. Apoptosis measured by AnnexinV staining in BTICs and non-BTICs with Mdivi-1 or DMSO vehicle treatment. Data are presented as mean ± s.e.m. (387: BTICs, $p < 0.0001$; non-BTICs, $p = 0.066$. 3565: BTICs, $p = 0.0005$; non-BTICS, $p = 0.5814$ by Student's t-test; ns = not significant; $n = 3$). **c**. Apoptosis was measured by Annexin V

staining in two human neural progenitor cell (NPC) lines (ENSA and 15167) with Mdivi-1 or DMSO treatment. Data are presented as mean ± s.e.m. (ENSA: p = 0.2571; 15167: p = 0.1413 by Student's t-test; ns = not significant; n = 3). **d**. Kaplan–Meier survival curves of immunocompromised mice bearing orthotopic 387 BTICs (3×10^5 cells/animal). Three days after tumor implantation, mice were treated with Midivi-1 (2.5 mg/kg) or DMSO vehicle control for 5 days (p = 0.0134 by log-rank analysis; n = 7).

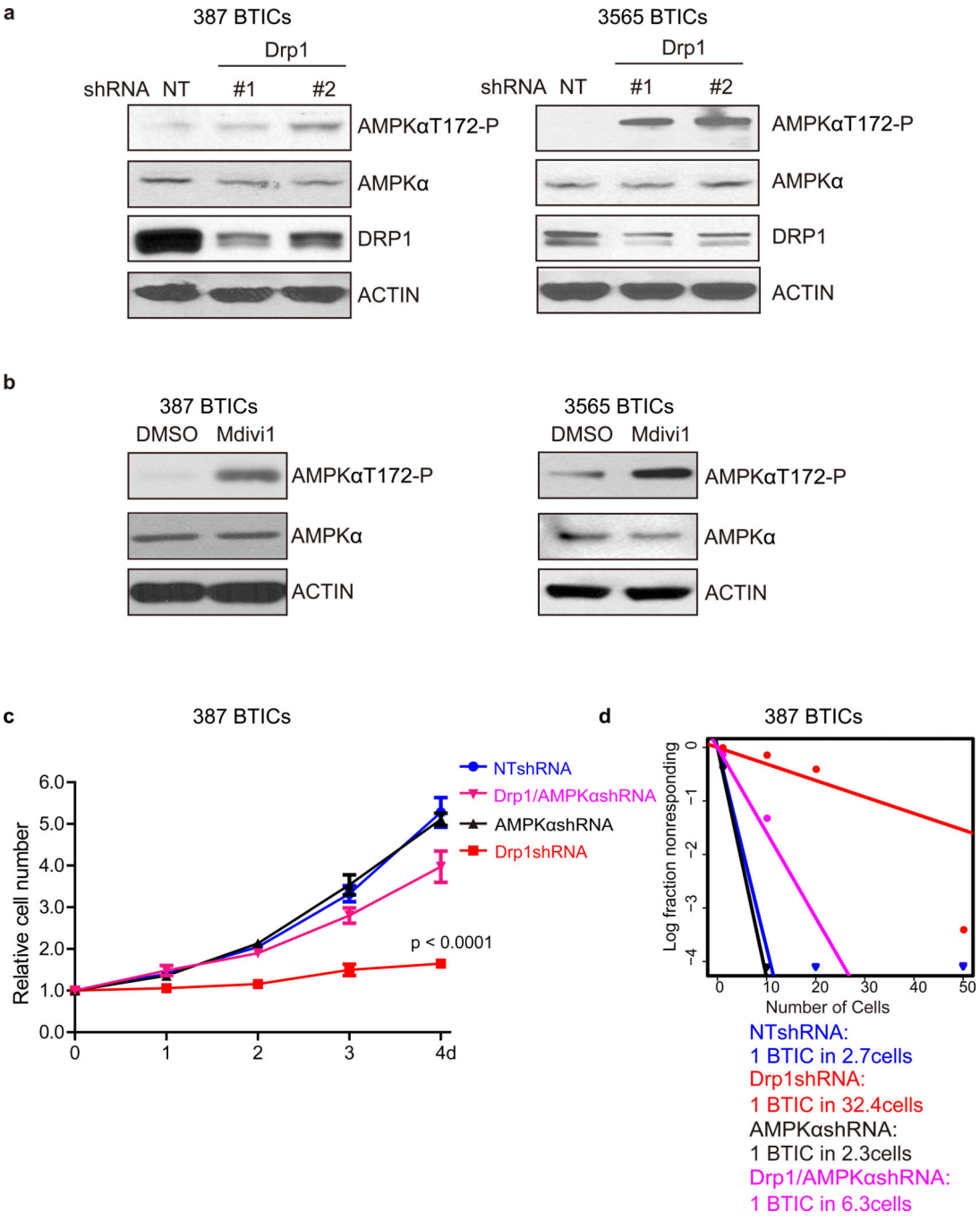

Figure 6. DRP1 inhibition induces AMPK activity in BTICs

a. Lysates of 387 and 3565 BTICs expressing NT control shRNA, shDrp1#1, or shDrp1#2 were immunoblotted with the indicated antibodies. shRNA mediated knockdown of DRP1 induced AMPK activity. Images were cropped for presentation. Full-length blots are presented in Supplementary Fig. 10. **b**. Lysates of 387 and 3565 BTICs treated with Midivi-1 or DMSO were immunoblotted with the indicated antibodies. Inhibition DRP1 by Midivi-1 induced AMPK activity. **c**. Growth curves of 387 BTICs expressing NT control shRNA, shDrp1, shAMPKα, or shDrp1 and shAMPKα together. Data are plotted as mean ±

s.e.m. $p < 0.0001$ by repeated measures ANOVA. **d**. In vitro extreme limiting dilution assays (ELDA) of 387 BTICs expressing NT control shRNA, shDrp1, shAMPKα, or shDrp1 and shAMPKα together. $p = 1.7 \times 10^{-34}$ by ANOVA.

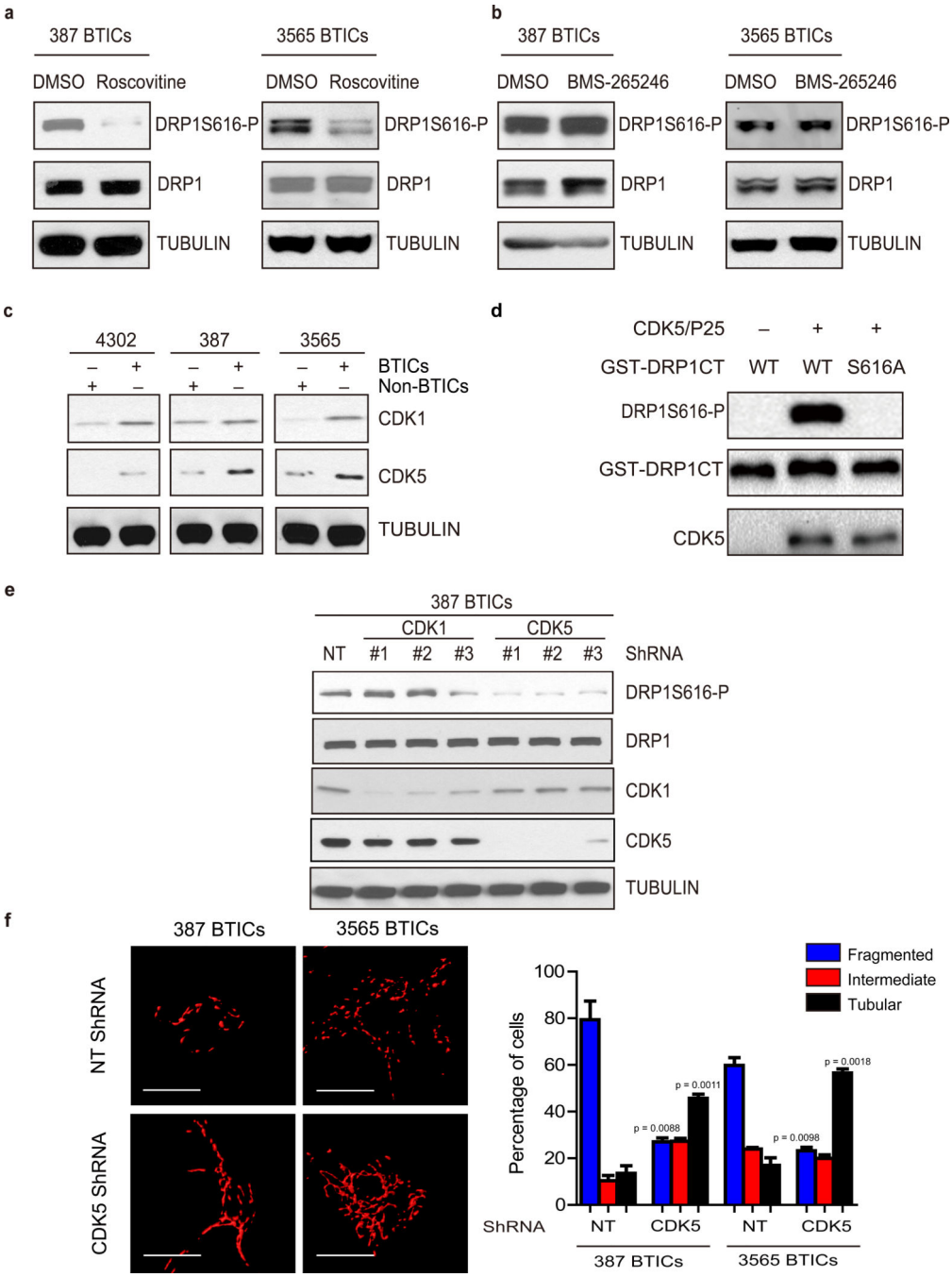

Figure 7. CDK5 activates DRP1 in brain tumor initiating cells

a. Lysates of 387 and 3565 brain tumor initiating cells (BTICs) treated with the CDK1/2/5 inhibitor Roscovitine or DMSO vehicle control were subjected to immunoblot analysis with the indicated antibodies. Images were cropped for presentation. Full-length blots are presented in Supplementary Fig. 11. **b**. Lysates of 387 and 3565 BTICs treated the CDK1/2 inhibitor BMS-265246 or DMSO were immunoblotted with the indicated antibodies. **c**. Immunoblot analysis of CDK1, CDK5, stem and differentiation markers in BTICs and non-BTICs isolated from multiple patient-derived glioma xenografts (4302, 387, and 3565). **d**. In

vitro kinase assays were performed with or without CDK5/p25 and either wild type or mutant (S616A) GST-C-terminal fragment of DRP1 (AA 518–736), GST-DRP1CT. **e**. Lysates of 387 BTICs expressing NT control shRNA or three independent shRNA constructs targeting CDK1 or CDK5 were immunoblotted with the indicated antibodies. Knockdown CDK5 but not CDK1 decreased phospho-DRP1^{S616} levels. **f**. Immunofluorescent staining of the mitochondrial marker TOM20 in 387 and 3565 BTICs expressing NT control shRNA or shCDK5. Data are represented as mean ± s.e.m. (387: fragmented, p = 0.0088; tubular, p = 0.0011. 3565: fragmented, p = 0.0098; tubular, p = 0.0018; Student's t-test; n = 3).

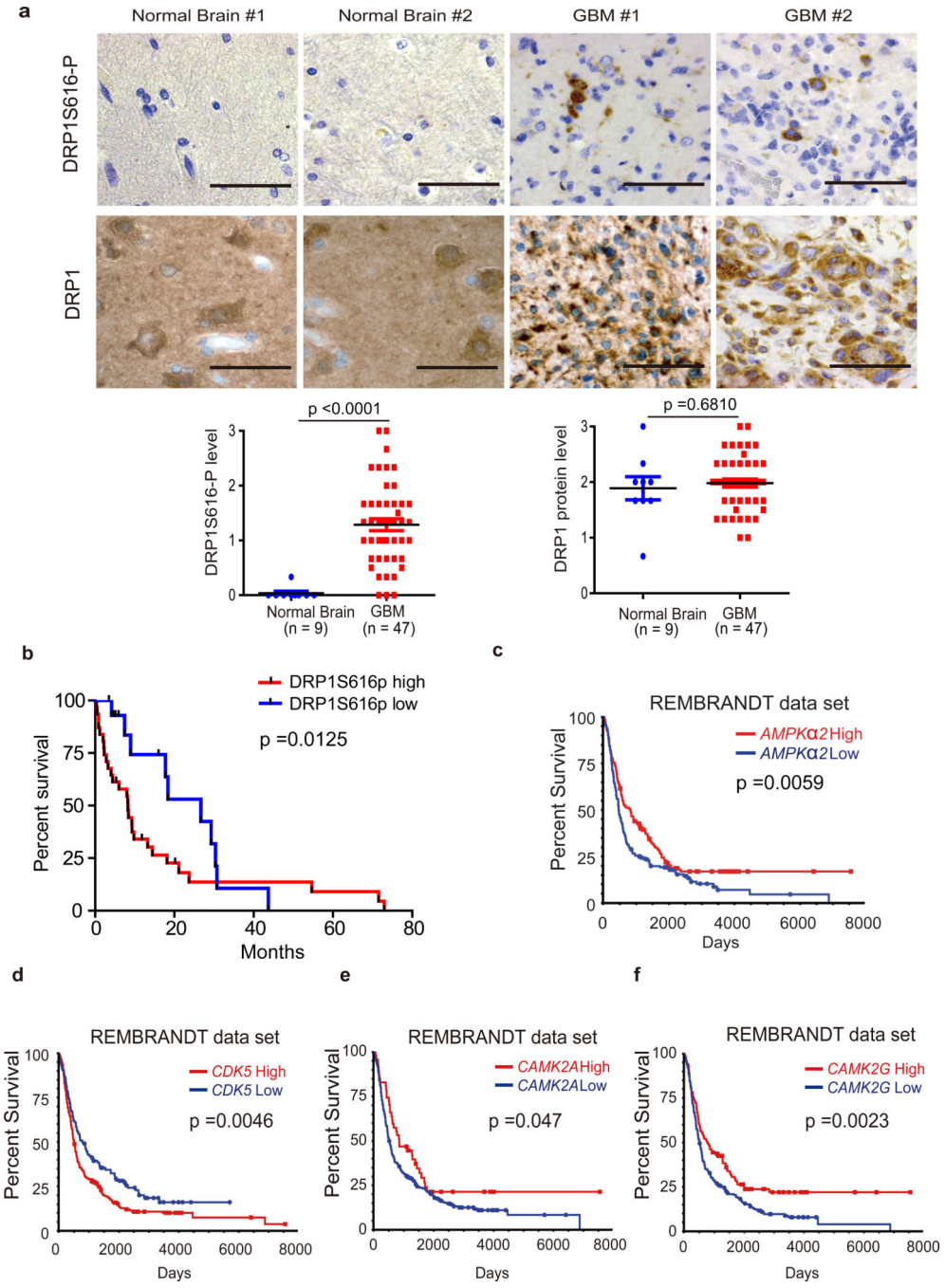

Figure 8. DRP1 regulation informs patient prognosis

a. Immunohistochemical (IHC) staining and scatter plot of DRP1 and phospho-DRP1^{S616} in human primary glioblastomas and non-neoplastic brain tissues in a tissue microarray. Scale bar, 50 μm. Phosphorylated DRP^{S616}: $p < 0.0001$; total DRP1: $p = 0.681$. **b**. Kaplan-Meier plot of tissue microarray data indicates that higher phosphorylation of DRP1 (phospho-DRP1^{S616}/total DRP1) correlates with poor glioblastoma patient survival. $p = 0.0125$ by log-rank analysis. **c**. Analysis of REMBRANDT data indicates that lower *AMPKA2* mRNA expression correlates with poor glioma patient survival. $p = 0.0059$ by log-rank analysis. **d–**

f. Analysis of REMBRANDT data indicates that higher CDK5 (p = 0.0046 by log-rank analysis) and lower *CAMK2* mRNA expression (p = 0.047 and 0.0023 by log-rank analysis for *CAMK2A* and *CAMK2G*, respectively) correlates with poor glioma patient survival.